10th Intern. Conf. on Indium Phosphide and Related Materials
11-15 May 1998 Tsukuba, Japan

EFFECTS OF AN InGaP ELECTRON BARRIER LAYER ON 1.55 μm LASER DIODE PERFORMANCE

P. Abraham, J. Piprek, S.P. DenBaars, J.E. Bowers
Electronic and Computer Engineering Department, University of California, Santa Barbara, CA 93106-9560 USA

Abstract

Temperature sensitive loss mechanisms are known to severely limit the performance of InGaAsP/InP laser diodes emitting at 1.55 μm. In this paper, we report on a simple modification of the classical InGaAsP laser structure to reduce electron leakage from the separate confinement heterostructure (SCH) layer.

I. Introduction

Lasers operating at 1.55 μm suffer from a low characteristic temperature of the threshold current T_0 and from a decrease of the external quantum efficiency when temperature increases. These two phenomena make it difficult to use long-wavelength lasers without thermo-electric coolers. The most commonly accepted reason of the low T_0 value is Auger recombination (1). The spill over of electrons from the separate confinement heterostructure (SCH), is the main reason of the decrease of the differential quantum efficiency when temperature increases (2). Different solutions were proposed to reduce this leakage. One is to introduce p doping at the p-cladding-SCH interface or even in the SCH. This is indeed an efficient way to increase the energy difference between the p-cladding and the active region conduction band. However, it also increases the internal loss. Another solution is to grow the structure in the InGaAlAs/InP system. It is then possible to take advantage of the type II interface between InP and InAlAs lattice matched to InP to introduce an electron barrier layer on the p side with AlInAs and a hole barrier layer on the n side with an InP layer (3). However, in that case the difficulty is in the growth of Al containing alloys. The typical oxygen concentration in MOCVD grown InAlAs is in the 10^{17} cm^{-3} to 10^{18} cm^{-3} range. It produces deep n type levels that increase the internal loss and the threshold current density. The internal loss and the threshold current density can be as high as 27 cm^{-1} and 1.1 kA/cm^2 for 6 QW GaInAlAs lasers (400 μm cavity length), respectively (4). In the InGaAsP system for the same number of wells and the same cavity length these values are of the order of 10 cm^{-1} and 0.7 kA/cm^2. An intermediate approach, utilizing InGaAsP QW and InGaAlAs barriers with an InAlAs electron stopper layer has also been investigated (5). In that case the internal losses are again in the 20 cm^{-1} range, but the electron stopper layer demonstrated to be efficient to decrease the leakage current.

In this paper, we report on a simple modification of the classical InGaAsP laser structure increasing the electron confinement in the SCH. A thin strained $In_{0.81}Ga_{0.19}P$ layer is inserted between the p-InP cladding layer and the SCH layer (Fig. 1). The conduction band energy of $In_{0.81}Ga_{0.19}P$ is about 50 meV higher than that of InP. The light hole (LH) band gap energy of $In_{0.81}Ga_{0.19}P$ on InP is almost the same as in InP. Thus, this layer does not hinder hole injection.

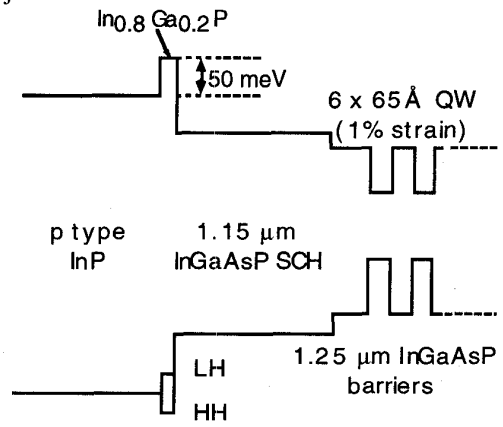

Fig. 1: Band structure of the active region with the InGaP electron stopper layer.

II. Experimental

The laser structure growth was performed in a Metalorganic Vapor Phase Epitaxy horizontal reactor made by Thomas Swan. The growth temperature and pressure were 645°C and 350 Torr, respectively. The

0-7803-4220-8/98/$10.00 ©1998 IEEE

sources were trimethylindium, trimethylgallium, tertiarybutylarsine and tertiarybutylphosphine.

The active region of the laser structures consists of six 6.5 nm wide 1%-compressive-strain QW's. The barriers are 5.5 nm thick and are made of lattice matched 1.25 μm wavelength InGaAsP (1.25 Q). The SCH is 300 nm thick with a 100 nm thick 1.25 Q region including the QW's embedded among two 100 nm thick 1.15 Q layers. The photoluminescence wavelength of structures with (W) and without (W/O) InGaP stopper layer are 1.49 μm and 1.5 μm, respectively. On the p side of the SCH the first 130 nm of the InP cladding layer were undoped to prevent back diffusion of Zn into the SCH thereby reducing the optical internal loss. The thickness of the $In_{0.81}Ga_{0.19}P$ layer is 6 nm in structure W. Broad area lasers with 50 μm large stripes were fabricated. The as-cleaved lasers were characterized under pulsed conditions (0.05 % duty cycle) for temperatures ranging from 290 to 390 K.

III. Results

Table 1 compares the properties of structures W and W/O. T_0 in that table was calculated for 700 μm long lasers for temperatures ranging between 20°C and 60°C. All the other characteristic properties are given at 20°C. It can be seen that the additional electron barrier has little effect on the laser properties listed in Table 1.

	Structure W/O	Structure W
η_i	0.69	0.67
α_i (cm^{-1})	9.7	11.2
J_{th} (A cm^{-2})	73	83
J_{tr} (A cm^{-2})	45	48
g_{th} (cm^{-1})	8.3	8.2
T_0 (K)	61	59

Table 1: Internal quantum efficiency η_i, internal loss α_i, threshold current density per QW J_{th}, transparency current density per QW J_{tr}, modal gain at threshold per QW of the laser structures W/O and W at 20°C.

The largest differences are in the internal loss and in the threshold current density that are respectively 15 % and 14 % higher in W than in W/O. T_0 is in the same range for both structures.

There is a critical temperature T_c that separates two regions where I_{th} and η_d have different temperature dependences (6). Table 2 shows the values of T_c and the characteristic temperatures T_0 and $T_{\eta d}$ above and below T_c for both structures for 250 μm long lasers. The way the differential quantum efficiency changes with respect to the temperature can be described by a characteristic temperature T_η. The relation used for the fit is

$$\eta_d = \eta_{d0} \exp(-T/T_{\eta d}) \qquad (1)$$

Structure W/O		Structure W	
$T_c \approx 370$ K		$T_c \approx 370$ K	
$T < T_c$	$T > T_c$	$T < T_c$	$T > T_c$
$T_0 = 52$K	$T_0 = 24$K	$T_0 = 48$K	$T_0 = 20$K
$T_{\eta\delta}$	$T_{\eta\delta}$	$T_{\eta\delta}$	$T_{\eta\delta}$
113 K	15 K	164 K	16 K

Table 2: Critical temperature T_c, characteristic temperature of the threshold current T_0 and of the differential quantum efficiency $T_{\eta d}$ below and above the critical temperature for 250 μm long laser structures W and W/O.

The only noticeable difference between the two structures is in $T_{\eta d}$ below T_c. It increases from 113 K to 164 K when adding the $In_{0.81}Ga_{0.19}P$ electron barrier layer whereas above T_c the $T_{\eta d}$ values are about the same. The improvement of $T_{\eta d}$ is observed whatever is the laser length. On contrary, T_0 (below T_c) of structures W and W/O follow the same trend and are close to each other for all the lengths measured.

The differential quantum efficiency η_d is related to the internal loss α_i and the internal quantum efficiency η_i by:

$$\frac{1}{\eta_d} = \frac{<\alpha_i>}{\eta_i \ln(1/R)} L + \frac{1}{\eta_i} \qquad (2)$$

where R is the mean reflection coefficient of the laser facets and L is its cavity length. Cavity lengths between 250 μm and 1 mm were utilized to calculate α_i and η_i using relation 2. The variation with temperature of α_i for both structures is very similar. It means that the higher value of $T_{\eta d}$ for structure W is essentially due to the higher value of the characteristic temperature of the internal quantum efficiency $T_{\eta i}$ (Fig. 2).

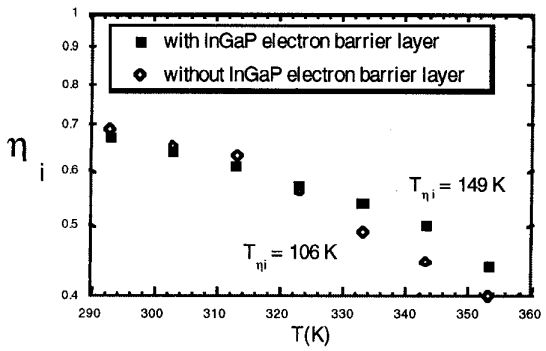

Fig. 2: Comparison of internal quantum efficency versus temperature measured with and without the InGaP electron barrier.

IV. Numerical Analysis

An advanced laser simulation software (7) is used to further analyze the effect of loss mechanisms on the high temperature performance of our laser diodes (T=353K). The software calculates the optical gain in strained quantum wells based on the 4x4 **kp** method including valence band mixing and carrier-carrier interaction. The computed photoluminescence spectrum as well as the gain peak wavelength agree well with our measured data. The magnitude of the gain is slightly adjusted to fit the measured threshold current of 380mA (laser length L=269µm, width W=57µm). The current calculation is based on a drift-diffusion model including thermionic emission at hetero barriers. Thermionic emission of electrons from the quantum wells causes a relevant leakage which can be identified as minority carrier current in the p-InP cladding layer. Carrier losses due to Auger recombination, spontaneous emission, and Shockley-Read-Hall (SRH) recombination are considered. Typical recombination parameters are assumed (8). The measured internal optical absorption α_i = 10cm^{-1} is applied in the simulation of the W/O laser and the calculated slope efficiency of 33% is in excellent agreement with the measurement. Introducing the InGaP stopper layer and increasing the absorption as measured (α_i = 13cm^{-1}) results in 30mA higher threshold current and an almost identical slope efficiency. Fig. 3 shows the band diagram in the center of the device including the InGaP layer (E_C – conduction band edge, E_V – valence band edge). The quasi-Fermi levels for electrons (F_n) and holes (F_p) are given at 510 mA injection current, well above threshold. For better comparison, this current level is maintained in the following figures. Fig. 4 displays the electron current density distribution $j_n(x)$ in the center of the device. Electrons are injected into the MQW from the n-InP on the left side and mostly recombine within the MQW.

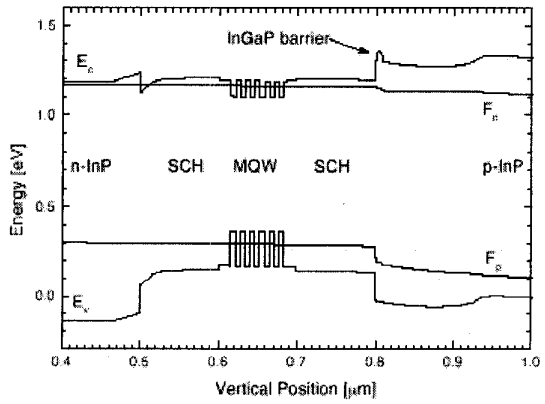

Fig. 3: Band diagram of the quantum well region of structure W.

But a small electron current remains on the right-hand-side in Fig. 4, indicating electron leakage into the p-InP cladding. With stopper layer, this leakage current is slightly smaller (solid line). From the leakage current increment per mA injection current, about 10% increase in differential injection efficiency η_i is attributed to the InGaP layer. Fig. 5 shows the electron density distribution n(x) in the center of the device. Introduction of the InGaP layer (solid line) causes a somewhat increased electron density which contributes to enhanced free carrier absorption. Higher absorption counteracts the improvement of the injection efficiency.

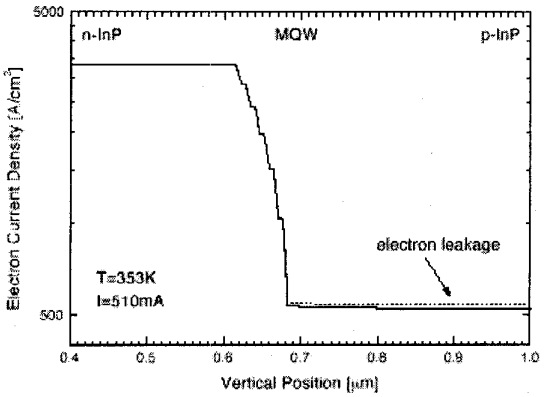

Fig. 4: Electron current density distribution in structure W (solid line) and W/O (dotted line). The horizontal axis is the same as for Fig. 3.

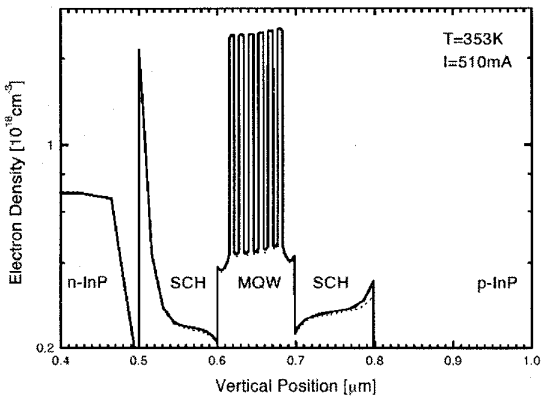

Fig. 5: Electron density distribution n(x) in the center of the device.

Assuming $\alpha_i = 10\ cm^{-1}$ in both simulations helps to reveal the pure impact of the stopper layer. Even without absorption increase, the threshold current is 10mA higher after introducing the stopper layer. The reason are slightly higher carrier densities in the quantum wells which are caused by a quasi-Fermi level shift at the stopper layer (see Fig. 3).

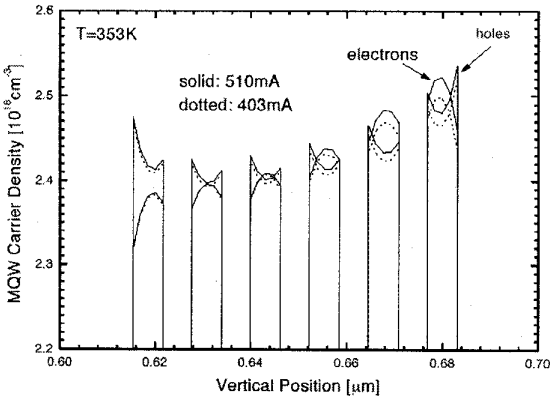

Fig. 6: QW carrier density of the structure W.

These higher QW densities lead to enhanced SRH- and Auger-recombination. Higher carrier densities also cause larger absorption (as measured). Since α_i is kept constant in this calculation, the computed slope efficiency η_d rises by about 1%. With optical losses being unchanged, this 1% improvement reflects the change in injection efficiency. But from our electron leakage investigation, about 10% improvement of η_i are expected. Some other carrier loss mechanism must counteract the reduced leakage. Usually, the QW carrier density is assumed to be clamped at the threshold level permitting no further increase in QW carrier losses. But the simulation reveals that this assumption is not correct in our case. Fig. 6 shows the electron and hole distribution with in the quantum wells at two different injection currents above threshold (structure W). The MQW carrier distribution is inhomogeneous because holes (injected from the right-hand-side) distribute not as easily as electrons. More importantly, the carrier density grows with injection current, causing higher recombination losses. Thus, the differential injection efficiency does not rise as much as expected from the suppressed electron leakage.

V. Conclusion

The introduction of an InGaP electron stopper layer in between the SCH and the p-InP cladding layer does not result in the expected improvement of threshold current. Improvements of differential quantum efficency and differential injection efficency are observed due to less electron leakage. Carrier losses within the quantum wells as well as internal absorption are found to counteract the reduced leakage.

References

(1) E.P. O'Reilly, G. Jones, M. Silver, A.R. Adams, "Determination of Gain and Loss Mechanisms in Semiconductors Lasers Using Pressure Techniques", Phys. Stat. Sol. B, vol. 198, pp. 363-3, 1996

(2) L. A. Coldren, S. W. Corzine, "Diode lasers and photonic integrated circuits", John Wiley & Sons, Inc, New York 1995

(3) R.F. Kazarinov, G.L. Belenky, "Novel Design of AlGaInAs-InP Lasers Operating at 1.3 μm", IEEE J. of Quantum Electr., vol. 31, pp. 423-426, 1995

(4) B. Borchert, R. Gessner, B. Stegmüller, "Advanced 1.55 μm Quantum-Well GaInAls Laser Diodes with Enhanced Performance", Jpn. J. Appl. Phys. vol. 33, pp. 1034-1039, 1994

(5) H. Murai, Y. Matsui, Y. Ogawa, T. Kunii, "Lasing Characteristics Under High Temperature Operation of 1.55 μm Strained InGaAsP/InGaAlAs MQW Laser with InAlAs Electron Stopper Layer", Electronics Letters, vol. 31, no. 24, pp. 2105-7, 1995

(6) S. Seki, H. Oohashi, T. Hirono, K. Yokoyama, "Study on the Dominant Mechanisms for the Temperature Sensitivity of Threshold Current in 1.3 μm InP-Based Strained-Layer Quantum-Well Lasers", IEEE Journal of Quantum Electronics, Vol. 32, pp. 1478-1485, 1996

(7) PICS3D by Crosslight Software Inc.

(8) J. Piprek, D. I. Babic, and J.E. Bowers, "Simulation and analysis of 1.55 μm VCSEL", J. Appl. Phys. vol. 81, pp. 3382-9, 1997.